Raman Scattering and Efficient UV Photoluminescence from Well-Aligned ZnO Nanowires Epitaxially Grown on GaN Buffer Layer

Hsin-Ming Cheng,[†,‡] Hsu-Cheng Hsu,[†] Yung-Kuan Tseng,[‡] Li-Jiaun Lin,[‡] and Wen-Feng Hsieh*,[†]

Department of Photonics and Institute of Electro-Optical Engineering, National Chiao Tung University, 1001 Tahsueh Road, Hsinchu 30050, Taiwan, Republic of China, and Material Research Laboratories, Industrial Technology Research Institute, Hsinchu 310, Taiwan, Republic of China

Received: December 15, 2004; In Final Form: February 24, 2005

Optical phonon confinement and efficient UV emission of ZnO nanowires were investigated in use of resonant Raman scattering (RRS) and photoluminescence (PL). The high-quality ZnO nanowires with diameters of 80−100 nm and lengths of several micrometers were epitaxially grown through a simple low-pressure vapor-phase deposition method at temperature 550 °C on the precoated GaN(0001) buffer layer. The increasing intensity ratio of *n*-order longitudinal optical (LO) phonon ($A_1(n\text{LO})/E_1(n\text{LO})$) with increasing scattering order in RRS reveals the phonon quantum confinement as shrinking the diameter of ZnO nanowires. The exciton-related recombination near the band-edge transition dominate the UV emissions at room temperature as well as at low temperature that exhibits almost no other nonstoichiometric defects in the ZnO nanowires.

I. Introduction

ZnO is a promising material for photonic devices in the wavelength range of ultraviolet to blue since it has a wide band gap energy of 3.37 eV and a large exciton binding energy of 60 meV at room temperature (RT). It is expected that exciton as well as polariton lasers will be fabricated using the ZnO-related materials and that they will overwhelm the GaN-related materials soon because excitonic-stimulated emission and optically pumped laser action in high-quality ZnO epitaxial films were observed[1,2] at room temperature. Because of the optical losses, including not only nonradiative recombination centers but also traps of excitons, the high quality of ZnO becomes even more imperative in the excitonic lasing process.

Recently, one-dimensional (1D) ZnO nanowire has attracted considerable attention owing to its good crystal quality and unique photonic properties.[3,4] ZnO nanowire is also expected to play an important role as crystal quality and photonic properties interconnect as functional units in the fabrication of electronic, optoelectronic, electrochemical, and electromechanical devices with nanoscale dimensions.[4−20] However, the synthesis of an array of well-aligned ZnO nanowires is of great interest because it is an imperative step to realize nanophotonic devices, which include light-emitting diodes and laser diodes. Different methods have been reported for fabricating arrays of well-aligned ZnO nanowires that include template methods,[20,21] vapor transports and condensation methods,[3,4] metal-organic source vapor deposition methods,[22,23] and buffer layer precoated methods.[18,24] The conductive ZnO buffer layer behaves as the nucleus for growth of wires in the meantime as the electrode for field-emission measurement.[18] Park et al.[19] also reported vertically aligned *n*-ZnO nanorods grown on the *p*-GaN surface. GaN has the same wurtzite-type structure as ZnO with a low

lattice mismatch (−1.9%). Therefore, ZnO nanowires on an epitaxial GaN buffer were expected to improve the crystal quality and to reduce the existence of structural defects. The *p−n* heterojunction of *n*-ZnO and *p*-GaN showed high current density and strong electroluminescence even at a low reversed bias voltage of 3 V. Accordingly, the buffer layer precoated method is a promising candidate for photonic device applications. This method has also been extensively used in epitaxial ZnO films,[25−28] but it was seldom used to grow ZnO nanowires.

In this letter, we report that vertical arrays of well-aligned ZnO nanowires were epitaxially fabricated on the GaN-buffered sapphire substrate by employing catalyst-free metal vapor deposition. We will discuss the interesting optical features of phonon quantum confinement and efficient UV emission in the use of Raman and photoluminescence (PL) spectroscopy. We also confirm a very small strain in the arrays of single-crystal ZnO nanowires by transmission electron microscopy (TEM) and high-resolution X-ray diffraction (HRXRD).

II. Experiments

Synthesis of the ZnO nanowire arrays was carried out in a low-pressure vapor-phase deposition system, which included a horizontal alumina tube in a conventional furnace. The zinc vapor source is 99.9% pure Zn metal powder from Strem Chemicals. High-quality epitaxial GaN(0001) buffer layers of up to 2-*μ*m thick were grown on (0001) sapphire substrates by metal−organic vapor-phase epitaxy (MOVPE). The GaN/sapphire substrates and zinc vapor source in an alumina boat were inserted into the quartz tube and placed closely to the middle of the furnace. Afterward, the chamber was heated to 550 °C at a rate of 20 °C/min under a constant flow of 55 sccm Ar and 1 sccm oxygen for 1 h. After cooling to ambient temperature, a white deposition layer was found over the substrate. More detailed growth conditions and the description of the reaction chamber are presented elsewhere.[24]

The as-synthesized products were characterized by field emission scanning electron microscopy (FESEM) [LEO-1530],

* To whom correspondence should be addressed. Tel: +886-3-5712121 ext. 56316; fax: +886-3-5716631; e-mail: wfhsieh@mail.nctu.edu.tw.
† National Chiao Tung University.
‡ Industrial Technology Research Institute.

which was equipped with an energy-dispersive spectroscopy (EDS) [EDAX] facility. The crystal structure of the nanowires was analyzed using a transmission electron microscope (TEM) [JEOL JEM-2000FX]. High-resolution X-ray diffraction (HRXRD) measurements were performed in a Bede D1 diffractometer equipped with a asymmetrically cut Si(220) monochromator and horizontal divergence slits with a width of 100 μm and a height of 2 mm to select the Cu $K_{\alpha1}$ radiation. An asymmetrically cut Si(220) analyzer crystal of 12 arcsec acceptance permitted the separation of mosaic tilt from strain.

Conventional and resonance Raman spectroscopy were carried out by a frequency-doubled Yb:YAG laser ($\lambda = 515$ nm) and a He–Cd laser ($\lambda = 325$ nm), respectively, and a Jobin–Yvon T64000 microspectrometer with a 1800 grooves/mm grating in the backscattering configuration was employed to investigate the lattice vibrational properties of the ZnO nanowires. A photoluminescence measurement was also made using a 20 mW He–Cd laser at wavelength of 325 nm, and the emitted light was dispersed by a TRIAX-320 spectrometer and detected by a UV-sensitive photomultiplier tube. A closed cycle refrigerator was used to maintain the measured temperature at 10 K.

III. Results and Discussion

The general morphology of ZnO nanowires was obtained using field emission scanning electron microscopy (FESEM). As shown in Figure 1, vertically well-aligned arrays of ZnO nanowires with high density ($\sim10^{10}$ cm^{-2}) were uniformly grown over the entire substrate. The length and diameter of the nanowires were controlled in the range between (2.8–3.0) μm and (80–100) nm, respectively. The EDS analyses showed that the nanowires are composed of Zn and O, while the element of Ga was also detected on the substrate. Further structural characterization of the ZnO nanowires was performed with TEM. Figure 2a displays the TEM image of a nanowire scratched from the substrate, and its selected area electron diffraction (SAED) pattern reveals the single-crystal wurtzite structure of the ZnO nanowire. From the high-resolution TEM (HRTEM) image in Figure 2b, we determined the lattice spacing to be 0.52 nm that corresponds to the d-spacing of (0002) crystal planes. The inset in Figure 2b displays the fast Fourier transform of the HRTEM image that confirms the ZnO nanowires are preferentially oriented in the c-axis direction.

Figure 3 shows the $\theta-2\theta$ X-ray diffraction patterns. Only the {0001} reflection family of ZnO, GaN, and the sapphire substrate appear in the wide-angle XRD profile of Figure 3a. Statistical evidence indicates that the epitaxial relationship between ZnO and GaN with the sapphire substrate would be $[0001]_{ZnO}$ // $[0001]_{GaN}$ // $[0001]_{\alpha-Al2O3}$ along the normal of the substrate, and $[10\bar{1}0]_{ZnO}$ // $[10\bar{1}0]_{GaN}$ // $[11\bar{2}0]_{\alpha-Al2O3}$ along the in-plane direction. More evidence of epitaxial growth was confirmed using the XRD phi-scan analysis, described in our previous report.[24] Meanwhile, the measurement of XRD θ-rocking curve was also performed to investigate the degree of alignment to the normal of the surface, as indicated in the inset of Figure 3a. It depicts that the θ-rocking curve of ZnO(0004) has a full width at half-maximum (fwhm) of 0.4°. The fwhm of ZnO nanowires grown on GaN-buffered c-plane sapphire was smaller than those directly grown on the c-plane sapphire without the buffer layer.[22] The narrow fwhm of the ZnO(0004) diffraction peak implies that the c-axes of nanowires are well oriented along the normal of the substrate surface but it is still 5 times larger than the (0004) peak of GaN buffer layer because of the tilt mosaic effects on ZnO nanowires. Since the similar mosaic structure can be easily observed for the epi-GaN layers,[29]
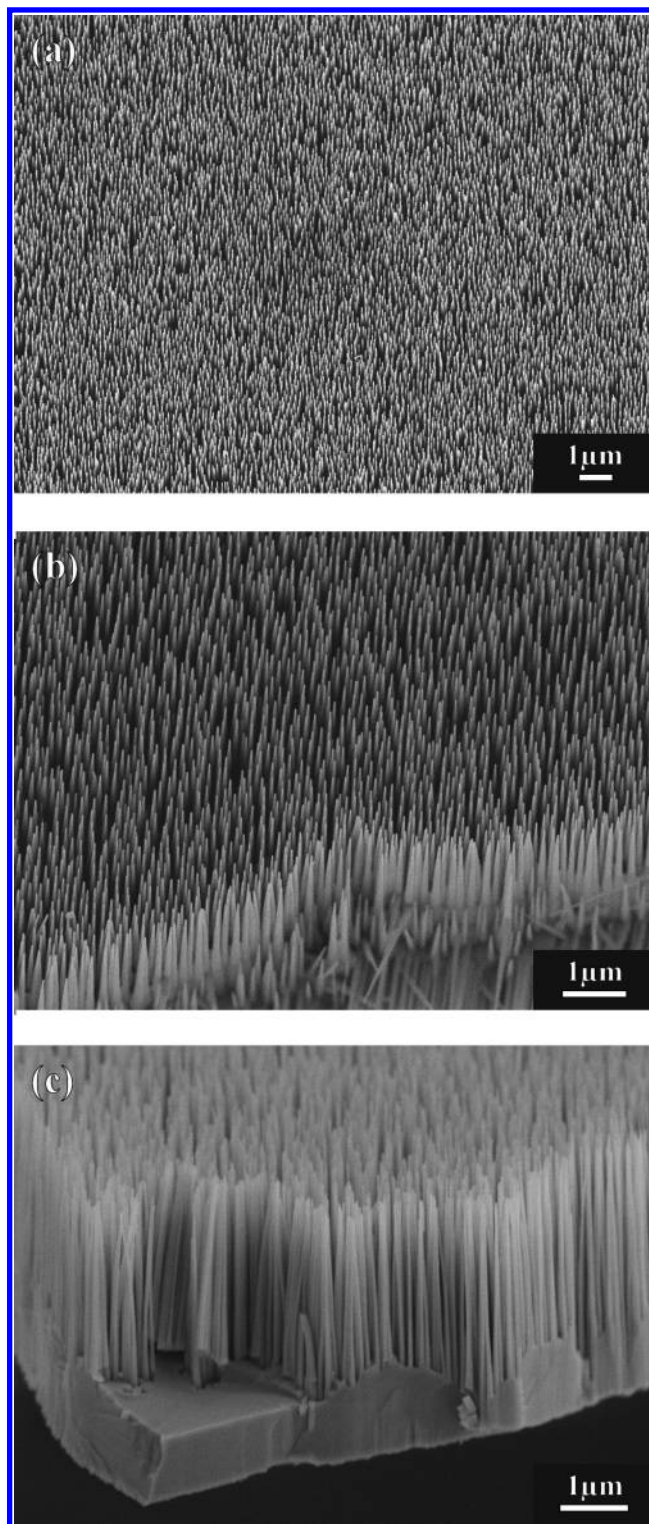

Figure 1. SEM images of vertically well-aligned ZnO nanowires grown on GaN-buffered sapphire substrate. (a, b) Large-scale and magnified SEM micrographs show the uniform 80–100 nm in diameter of ZnO nanowires and (c) cross-sectional image shows the length about 3.0 μm.

the quality of the ZnO nanowires grown on epi-GaN is basically limited by the quality of epi-GaN used as the buffer layer or even worse. The HRXRD pattern shown in Figure 3b demonstrates the strongly reflected GaN(0004) diffraction peak and the relatively weak ZnO(0004) peak, separately. However, the position of ZnO(0004) peak at 72.541° corresponds to $c = 5.208$Å, which slightly differs from that of the strain-free ZnO

Raman Scattering and Efficient UV Photoluminescence

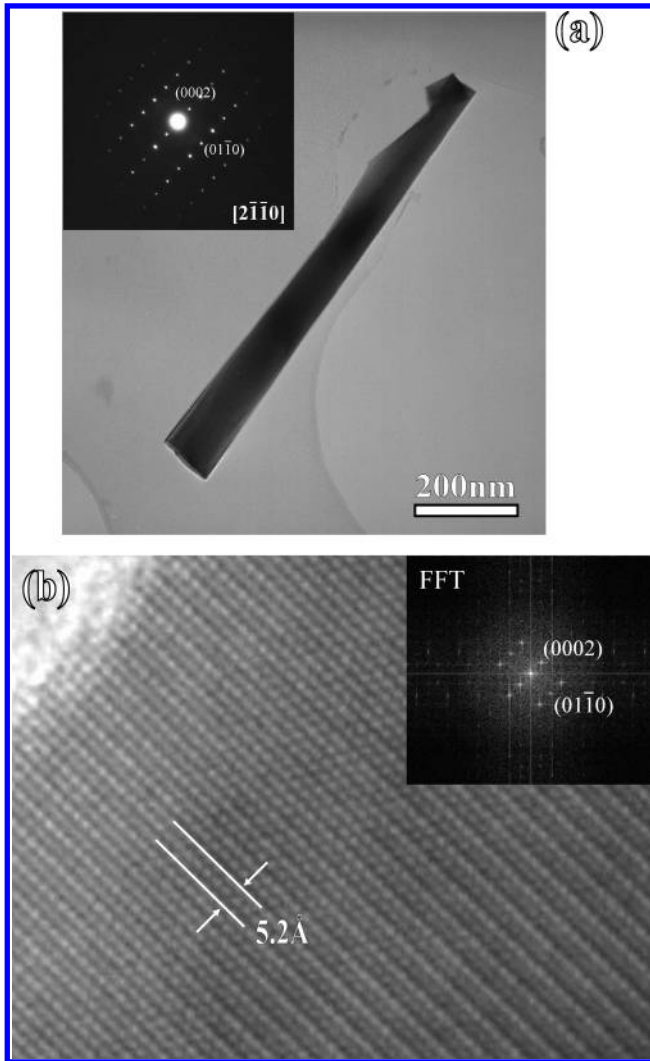*J. Phys. Chem. B, Vol. 109, No. 18, 2005* **8751**

Figure 2. (a) TEM image of wurtzite structure ZnO nanowire and the corresponding electron diffraction pattern (inset). (b) HRTEM image with inset of its corresponding FFT pattern.

powder[30] with $c = 5.206$Å. The wurzite ZnO crystal would be elongated along the c-axis under a tensile strain in c-plane.

To further explore the strain in ZnO nanowires, reciprocal space mapping (RSM) was carried out to determine a and c lattice parameters of ZnO nanowires. Figure 4 shows the RSM of the asymmetric (20$\bar{2}$4) reflection of the arrays of ZnO nanowires and the epi-GaN buffer layer. The reflection of the underlying GaN template has always been used as a reference and therefore the points in reciprocal space are given by l and k in units of the reciprocal vectors of GaN, $[0001]_{GaN}$, and $[10\bar{1}0]_{GaN}$, respectively. For the wurtzite materials such as GaN and ZnO, the magnitudes of these vectors are $|[0001]| = (2\pi/c)$ and $|[10\bar{1}0]| = (4\pi/\sqrt{3}a)$, which unambiguously determine the correlation between the values of l and k and the lattice constants c and a in real space, respectively. Because the GaN buffer layer has $c_{GaN} = 5.192$ Å and $a_{GaN} = 3.188$ Å, which is also strained by the sapphire substrate, the lattice constants of ZnO nanowires in the arrays can be estimated to be $c_{ZnO} = 5.208$ Å and $a_{ZnO} = 3.248$ Å by use of the relationships: $l^*|[0001]_{GaN}| = (2\pi)/(c_{ZnO}/4)$ and $h^*|[10\bar{1}0]_{GaN}| = (4\pi)/(\sqrt{3}a_{ZnO}/2)$. The lattice constants slightly differ from those of the strain-free ZnO powder,[30] which has $c_o = 5.2066$Å and $a_o = 3.2498$Å; thus, the strains $\epsilon_{zz} = \epsilon_{cc} = (c - c_o)/c_o > 0$ and $\epsilon_{xx} = \epsilon_{aa} = (a - a_o)/a_o < 0$, indicate a biaxial compressive strain in the a-plane, and an uniaxial tensile strain along the c-axis.
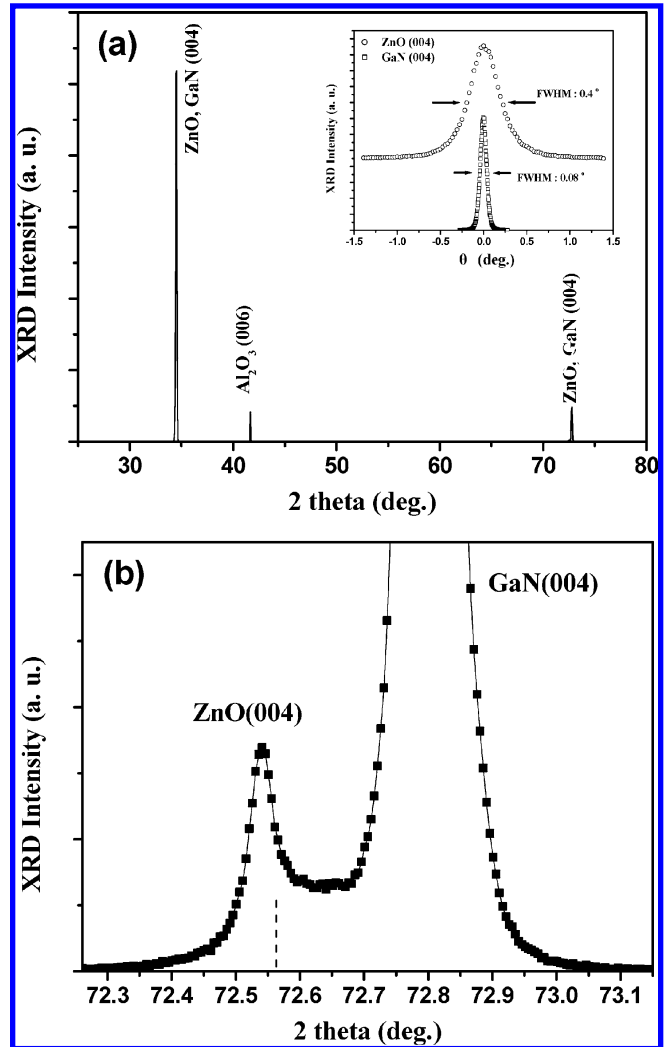

Figure 3. (a) $\theta-2\theta$ XRD profile of ZnO nanowires on epi-GaN(001)/α-Al$_2$O$_3$(001). The inset depicts the θ-rocking curves of ZnO(004) and GaN(004), respectively. (b) HRXRD shows the (004) reflection of ZnO nanowires slightly shift from that of the strain-free ZnO powder (dash line).
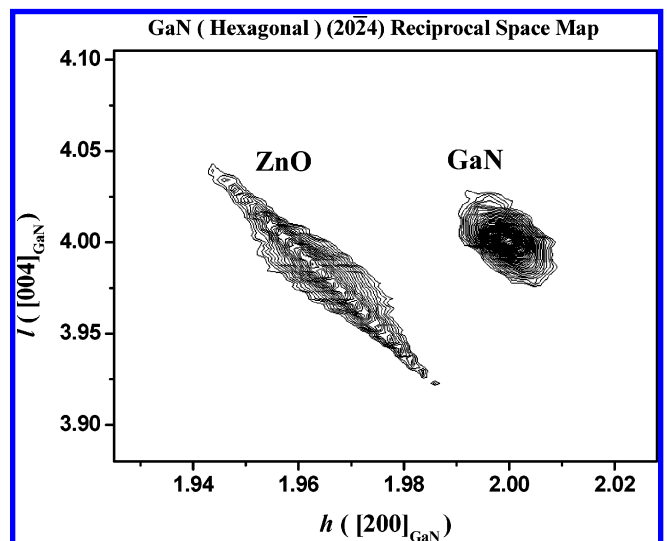

Figure 4. Reciprocal space map of asymmetric (20$\bar{2}$4) diffraction spots of a ZnO nanowires and epi-GaN buffer layer. The intensities are plotted logarithmically.

Since the thermal expansion coefficient of ZnO ($6.51 \times 10^{-6}/$K) is a little distinct from that of GaN ($5.59 \times 10^{-6}/$K)[28] and

8752 *J. Phys. Chem. B, Vol. 109, No. 18, 2005*

Cheng et al.

the reaction occurs at the low temperature of 550 °C, it is expected that the strain comes from the nature lattice misfit between ZnO and GaN. The residual in-plane biaxial stress can be obtained via the equation[31]

$$\sigma = -453.6 \times 10^9 \, \epsilon_{zz} \qquad (1)$$

It can thus be calculated that the arrays of ZnO nanowires have a compressive stress of −121.9 MPa when using the strain value $\epsilon_{zz} = 0.0269\%$, which is quite smaller than that of ZnO nanowires grown on other substrates.[32]

The UV Raman scattering was performed to investigate the vibrational properties of the arrays of ZnO nanowires at room temperature. Since the wurtzite structure of ZnO and GaN belongs to the space group C_{6v}^4($P6_3$mc), one primitive cell includes two formula units, with all of the atoms occupying $2b$ sites of symmetry C_{3v}. Group theory predicts the existence of the following optic modes: $A_1 + 2B_1 + E_1 + 2E_2$ at the Γ point of the Brillouin zone; B_1(low) and B_1(high) modes are normally silent; A_1, E_1, and E_2 modes are Raman active; and A_1 and E_1 are also infrared active. Thus, A_1 and E_1 are split into longitudinal (LO) and transverse (TO) optical components. Figure 5a shows a normal Raman spectrum of the ZnO nanowires which was taken with an accumulation time of 300 s from a 1 μm^2 spot size excited by a frequency-doubled Yb: YAG laser ($\lambda = 515$ nm). As we can see, the remarkable E_2-(high) mode of ZnO is located at 437 cm^{-1}; the weak and almost invisible signal around 580 cm^{-1} is contributed to the A_1(LO) and E_1(LO); and the E_1(TO), E_2(high), and A_1(LO) modes that belong to the epi-GaN buffer layer were also observed at 559, 569, and 737 cm^{-1}, respectively, because of the penetration of 515-nm laser light. In the backscattering geometry, the E_1(LO) mode is theoretically forbidden according to the Raman selection rules, however, it can be still visible if the incident direction of the excited light beam with respect to the crystal axes is not well-defined in the use of the focusing lens for micro-Raman measurement, and thus mixed modes may be observed. Furthermore, the bending and the tilting of ZnO nanowires may probably cause the appearance of the E_1(LO) mode.

For the advanced study, we used a He−Cd laser ($\lambda = 325$ nm) as the excitation source. In resonant Raman scattering (RRS), the exciting photon energy is resonant with the electronic interband transition energy of the wurtzite ZnO. The polar symmetry makes the A_1(LO) and E_1(LO) modes the dominant modes and it may exhibit different frequencies from the transverse optic (TO) modes. An intense multiphonon scattering was observed in the resonant Raman spectrum of Figure 5b, where four major bands were observed, centered at 577, 1154, 1729, and 2300 cm^{-1}, with bandwidths of 28, 49, 58, and 62 cm^{-1}, respectively, which mainly result from the polar symmetry modes A_1(LO) and E_1(LO) and their overtones. The first-order Raman mode at 577 cm^{-1} is a superposition of the A_1(LO) mode at 574 cm^{-1} and the E_1(LO) mode at 583 cm^{-1} in which Zn atoms and O atoms have the same vibration direction, respectively, to the neighbor lattices of the wurtzite ZnO.[33] The weak peak, around 437 cm^{-1}, which is contributed to the E_2(high) mode around 437 cm^{-1}, is almost imperceptible as a result of other (overlapping/stronger) RRS peaks. The absence of the TO modes could be attributed to the special angle between the wave vector of photons and the c-axis of the wurzite ZnO crystals in the near backscattering geometry employed in our measurement.

Multiphonon scattering processes have also been previously reported for single crystalline bulk ZnO,[34] and recently for ZnO films,[35] ZnO-opal structures,[36] and ZnO nanowires grown on m-sapphire.[37] The line widths of multiphonon scatterings cannot
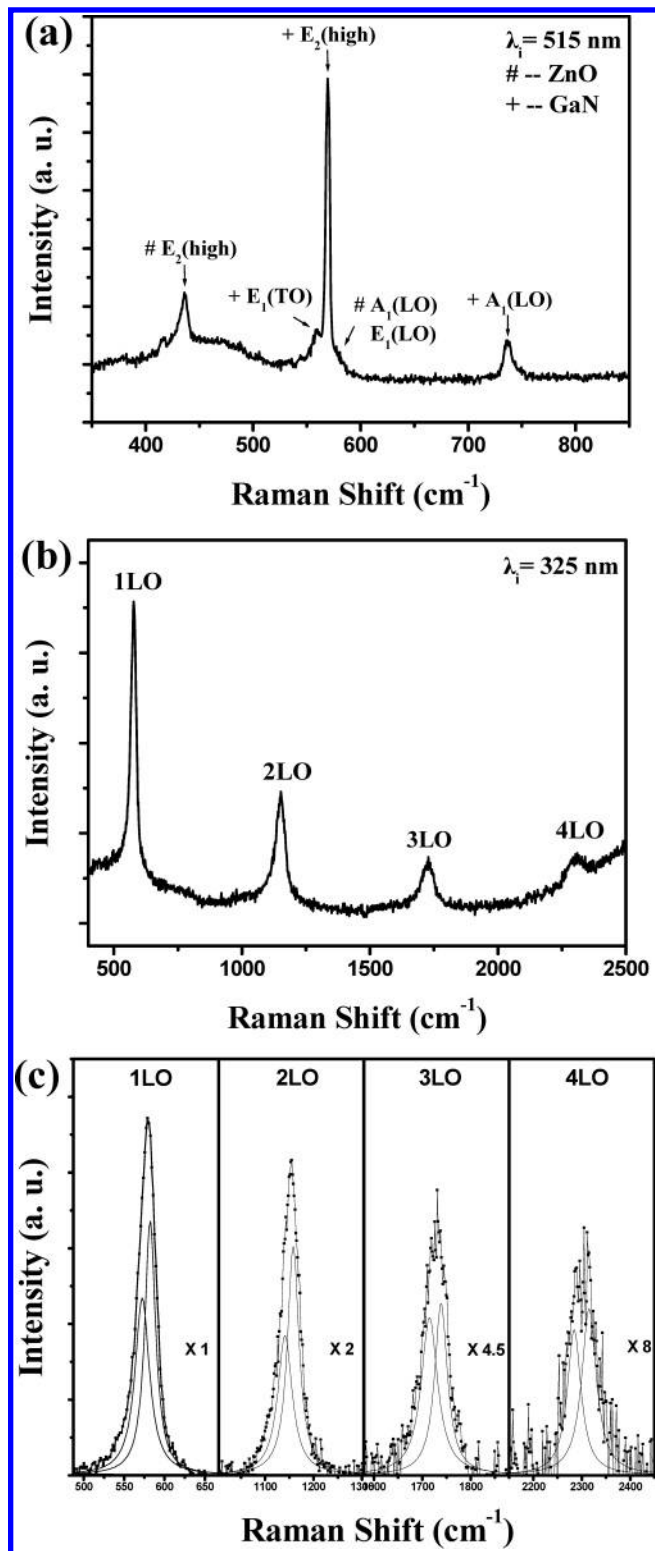

Figure 5. (a) Conventional Raman spectrum of ZnO nanowires on GaN buffer layer at room temperature using a frequency-doubled Yb: YAG laser ($\lambda = 515$ nm). (b) Resonant Raman scatterings (RRS) of ZnO nanowires on GaN buffer layer using a He−Cd laser ($\lambda = 325$ nm). The nLO refers to the nth longitudinal optical phonon. (c) Fitting profile of RRS spectrum and its decomposition. The scatter lines represent the recorded nLO RRS, and the solid lines are its decomposition which indicate A_1(nLO) and E_1(nLO), respectively.

be explained by the equation[34] σ (nLO) = 9n (cm^{-1}). The observed broadening of phonon line width is attributed to the phonon quantum confinement in ZnO nanowires. A similar broadening effect has also been observed in ZnO nanoparticles[38]

Raman Scattering and Efficient UV Photoluminescence

J. Phys. Chem. B, Vol. 109, No. 18, 2005 **8753**

and in ZnO nanowires,[37] which were grown on an m-sapphire substrate. Careful analysis of the resonant Raman spectrum was performed by the peak fitting, as shown in Figure 5c. The luminescence baseline was first removed and double Lorentzian profiles were chosen to fit the individual peaks of $A_1(n\text{LO})$ and $E_1(n\text{LO})$. The results of curve fitting give the multiphonon scattering of $A_1(n\text{LO})$ located at 571, 1139, 1713, and 2282 cm^{-1}, with the multiphonon scattering of $E_1(n\text{LO})$ located at 581, 1156, 1737, and 2313 cm^{-1}. The intensity ratio of $A_1(n\text{LO})/E_1(n\text{LO})$ was obviously increased for the higher order phonon scattering. Because the atoms in the E_1 mode displace along the a-axis, they could be easily restrained with the degrees of freedom defined by the cross section of ZnO nanowires. On the contrary, the A_1 mode is less affected by shrinking the diameter of ZnO wires because of its vibration along the c-axis. Accordingly, the intensity ratio of A_1/E_1 increases as the order of phonon scattering is increased. It is again further evidence of the phonon quantum confinement in ZnO nanowires.

Figure 6a shows a typical PL spectrum taken at room temperature, which consists of a strong UV peak at 3.26 eV and relatively no other visible emission. The UV band was attributed to the exciton-related emission near the band-edge, usually reported as the recombination of free excitons. The strong UV emission with no visible band in the PL spectra indicates that the ZnO nanowires grown on GaN have a good crystal quality with few nonstoichiometric defects. To investigate the UV emission in more detail, Figure 6b shows the low-temperature photoluminescence (LTPL) spectra measured at $T = 10$ K under various laser intensities. The excitation intensities were set from 0.05 Wcm^{-2} to 12 Wcm^{-2}. The bound exciton peak situated at 3.343 eV is predominant with its longitudinal (LO) phonon replicas at the lower energy side. In the inset of Figure 6b, other than this dominant peak that has been previously reported as the recombination of excitons bound to neutral donors or acceptors,[39,40] there is an additional weak feature situated on the high-energy shoulder around 3.364 eV. This higher energy emission is attributed to the donor-bound exciton (D°X) which is usually observed in ZnO single crystals,[41] epitaxial layers,[42] and other reports of 1-D ZnO rods and wires.[20,43]

With an increase in excitation intensity, we observed a remarkable increase in the PL intensity, with neither a blue nor a red shift. The variation of the integrated emission intensity versus the excitation laser intensity can be fitted to the simple power law: $I \propto L^{\gamma}$, as shown in Figure 6c, where I is the PL intensity, L is the excitation laser intensity, and γ is a dimensionless exponent. The integrated intensity of the PL band increases superlinearly with the excitation intensity, with $\gamma = 1.039$ and 1.015 for the 3.343 and 3.364 eV peaks, respectively. The exponent γ generally lies between 1 and 2 for the free- and bound-exciton emission and is less than or equal to 1 for free-to-bound and donor−acceptor pair recombinations.[44] The obtained values of $\gamma = 1.039$ and 1.015 confirm our assignment that the observed UV emission bands of ZnO nanowires are due to excitonic emissions.

IV. Conclusion

High-density, vertically oriented arrays of ZnO nanowires were successfully epitaxial grown on the GaN(0001)-buffered sapphire substrate without any catalyst. FESEM micrographs demonstrate that the ZnO nanowires possess a good crystalline structure with diameters of 80−100 nm and lengths of several micrometers. TEM micrograph and HRXRD spectra demonstrate that the arrays of ZnO nanowires are well aligned along
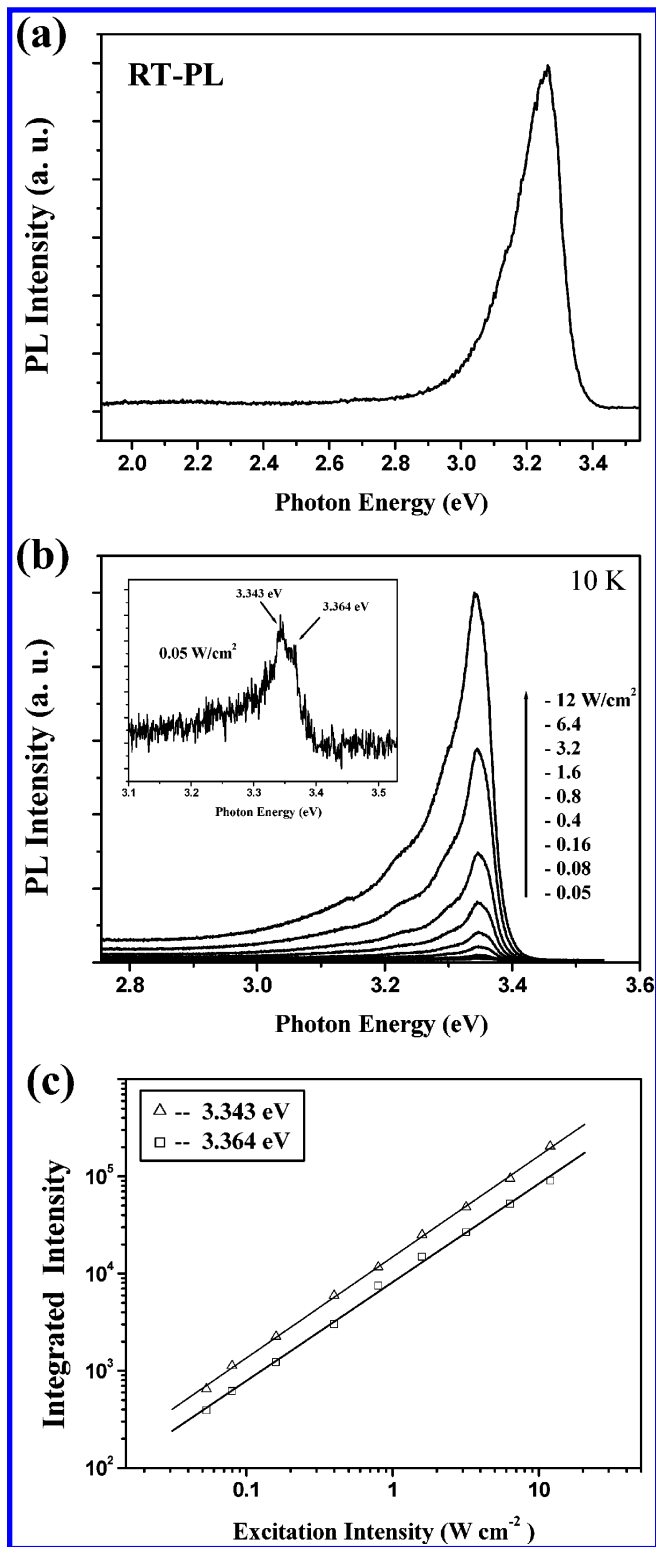

Figure 6. (a) Room-temperature photoluminescence (PL) spectrum of ZnO nanowires on GaN buffer layer. (b) PL spectra of ZnO nanowires as a function of excitation laser intensity (from 0.05 Wcm^{-2} to 12 Wcm^{-2}) at low temperature $T = 10$ K. (c) Dependence of integrated PL band intensity of 3.343 eV and 3.364 eV on excitation laser intensity at $T = 10$ K.

the c-axis and suffer a small biaxial compressive stress of 121.9 MPa. The resonant Raman spectra show good crystal quality and reveal phonon modes that are affected by the size confinement of the ZnO nanowire. Room-temperature and low-temperature photoluminescence exhibit almost no nonstoichiometric defects in the crystallite. The exciton-related recombi-

nations near the band edge dominate the UV emissions at room temperature as well as at low temperature ($T = 10$ K).

References and Notes

(1) Zu, P.; Tang, Z. K.; Yu, P.; Wong, G. K. L.; Kawasaki, M.; Ohtomo, A.; Koinuma, H.; Segawa, Y. *Solid State Commun.* **1997**, *103*, 459.

(2) Bagnall, D. M.; Chen, Y. F.; Zhu, Z. Q.; Yao, T.; Koyama, S.; Shen, M. Y.; Goto, T. *Appl. Phys. Lett.* **1997**, *70*, 2230.

(3) Huang, M. H.; Wu, Y.; Feick, H.; Tran, N.; Weber, E.; Yang, P. *Adv. Mater.* **2001**, *13*, 113.

(4) Huang, M. H.; Mao, S.; Feick, H.; Yan, H.; Wu, Y.; Kind, H.; Weber, E.; Russo, R.; Yang, P. *Science* **2001**, *292*, 1897.

(5) Law, M.; Sirbuly, D.; Johnson, J.; Goldberger, J.; Saykally, R.; Yang, P. *Science* **2004**, *305*, 1269.

(6) Johnson, J. C.; Yan, H. Q.; Yang, P. D.; Saykally, R. J. *J. Phys. Chem. B* **2003**, *107*, 8816.

(7) Yan, H.; Justin, J.; Law, M.; Saykally, R.; Yang, P. *Adv. Mater.* **2003**, *15*, 1907.

(8) Johnson, J. C.; Knutsen, K. P.; Yan, H.; Law, M.; Yang, P.; Saykally, R. *Nano. Lett.* **2004**, *4*, 197.

(9) Bai, X. D.; Gao, P. X.; Wang, Z. L.; Wang, E. G. *Appl. Phys. Lett.* **2003**, *82*, 4806.

(10) Bai, X. D.; Wang, E. G.; Gao, P. X.; Wang, Z. L. *Nano. Lett.* **2003**, *3*, 1147.

(11) Kong, X. Y.; Wang, Z. L. *Nano Lett.* **2003**, *3*, 1625.

(12) Arnold, M.; Avouris, P.; Pan, Z. W.; Wang, Z. L. *J. Phys. Chem. B* **2003**, *107*, 659.

(13) Kong, X. Y.; Ding, Y.; Yang, R. S.; Wang, Z. L. *Science* **2004**, *303*, 1348.

(14) Kong, X. Y.; Wang, Z. L. *Appl. Phys. Lett.* **2004**, *84*, 975.

(15) Hughes, W. L.; Wang, Z. L. *J. Am. Chem. Soc.* **2004**, *126*, 6703.

(16) Zhao, M. H.; Wang, Z. L.; Mao, S. X. *Nano Lett.* **2004**, *4*, 587.

(17) Liu, C. H.; Zapien, J. A.; Yao, Y.; Meng, X. M.; Lee, C. S.; Fan, S. S.; Lifshitz, Y.; Lee, S. T. *Adv. Mater.* **2003**, *15*, 838.

(18) Tseng, Y. K.; Huang, C. J.; Cheng, H. M.; Lin, I. N.; Liu, K. S.; Chen, I. C. *Adv. Funct. Mater.* **2003**, *13*, 811.

(19) Park, W. I.; Yi, G. C. *Adv. Mater.* **2004**, *16*, 87.

(20) Park, W. I.; Jun, Y. H.; Jung, S. W.; Yi, G. C. *Appl. Phys. Lett.* **2003**, *82*, 964.

(21) Zheng, M. J.; Zhang, L. D.; Li, G. H.; Shen, W. Z. *Chem. Phys. Lett.* **2002**, *363*, 123.

(22) Park, W. I.; Kim, D. H.; Jung, S.-W.; Yi, G.-C. *Appl. Phys. Lett.* **2002**, *80*, 4232.

(23) Wu, J. J.; Liu, S.-C. *Adv. Mater.* **2002**, *14*, 215.

(24) Tseng, Y. K.; Chia, C. T.; Tsay, C. Y.; Lin, L. J.; Cheng, H. M.; Kwo, C. Y.; Chen, I. C. *J. Electrochem. Soc.* **2005**, *152*, G95.

(25) Ko, H. J.; Chen, Y. F.; Yao, T.; Miyajima, K.; Yamamoto, A.; Goto, T. *Appl. Phys. Lett.* **2000**, *77*, 537.

(26) Ko, H. J.; Chen, Y. F.; Hong, S. K.; Wenisch, H.; Yao, T.; Look, D. C. *Appl. Phys. Lett.* **2000**, *77*, 3761.

(27) Nahhas, A.; Kim, H. K.; Blachere, J. *Appl. Phys. Lett.* **2001**, *78*, 1511.

(28) Vispute, R. D.; Talyansky, V.; Choopun, S.; Sharma, R. P.; Venkatesan, T.; He, M.; Tang, X.; Halpern, J. B.; Spencer, M. G.; Li, Y. X.; Salamanca-Riba, L. G.; Iliadis, A. A.; Jones, K. A. *Appl. Phys. Lett.* **1998**, *73*, 348.

(29) Potin, V.; Ruterana, P.; Nouet, G.; Pond, R. C.; Morkoç, H. *Phys. Rev. B* **2000**, *61*, 5587.

(30) McMurdie, H.; Morris, M.; Evans, E.; Paretzkin, B.; Wong-Ng, W.; Ettlinger, L.; Hubbard, C. *Powder Diffr.* **1986**, *1*, 76.

(31) Puchert, M. K.; Timbrell, P. Y.; Lamb, R. N. *J. Vac. Sci. Technol. A* **1996**, *14*, 2220.

(32) Zhang, Y.; Jia, H.; Wang, R.; Chen, C.; Luo, X.; Yu, D.; Lee C. *Appl. Phys. Lett.* **2003**, *83*, 4631.

(33) Damen, T. C.; Porto, S. P. S.; Tell, B. *Phys. Rev.* **1966**, *142*, 570.

(34) Scott, J. F. *Phys. Rev. B* **1970**, *2*, 1209.

(35) Zhang, X. T.; Liu, Y. C.; Zhi, Z. Z.; Zhang, J. Y.; Lu, Y. M.; Shen, D. Z.; Xu, W.; Zhong, G. Z.; Fan, X. W.; Kong, X. G. *J. Phys. D* **2001**, *34*, 3430.

(36) Ursaki, V. V.; Tiginyanu, I. M.; Zalamai, V. V.; Masalov, V. M.; Samarov, E. N.; Emelchenko, G. A.; Briones, F. *J. Appl. Phys.* **2004**, *96*, 1001.

(37) Ng, H. T.; Chen, B.; Li, J.; Han, J.; Meyyappan, M.; Wu, J.; Li, S. X.; Haller, E. E. *Appl. Phys. Lett.* **2003**, *82*, 2023.

(38) Rajalakshmi, M.; Aror, A. K.; Bendre, B. S.; Mahamuni, S. *J. Appl. Phys.* **2000**, *87*, 2445.

(39) Reynolds, D. C.; Litton, C. W.; Collins, T. C. *Phys. Rev.* **1965**, *140*, A1726.

(40) Chen, Y. F.; Bagnall, D. M.; Koh, K. O.; Park, K. T.; Hiraga, K.; Zhu, Z.; Yao, T. *J. Appl. Phys.* **1998**, *84*, 3912.

(41) Chichibu, S. F.; Sota, T.; Cantwell, G.; Eason, D. B.; Litton, C. W. *J. Appl. Phys.* **2003**, *93*, 756.

(42) Jung, S. W.; Park, W. I.; Cheong, H. D.; Yi, G.-C.; Jang, H. M. *Appl. Phys. Lett.* **2002**, *80*, 1924.

(43) Hsu, H. C.; Tseng, Y. K.; Cheng, H. M.; Kuo, J. H.; Hsieh W. F. *J. Cryst. Growth* **2004**, *261*, 520.

(44) Schmidt, T,; Lischka, K.; Zulehner, W. *Phys. Rev. B* **1992**, *45*, 8989.